Pergamon

Journal of Structural Geology, Vol. 17, No. 5, pp. 631 to 646, 1995

0191-8141/95 $9.50+0.00

0191-8141(94)00094-8

Numerical modeling of propagation and overlap of thrust faults, with application to the thrust-fold belt of central Alberta

D. LEBEL* and E. W. MOUNTJOY

Department of Earth and Planetary Sciences, McGill University, 3450, University Street, Montréal, Québec, Canada, H3A 2A7

(*Received* 1 *November* 1993; *accepted in revised form* 12 *August* 1994)

Abstract—We use two computer programs to analyze the propagation of multiple thrust faults and their influence on the geometry of a thrust belt. They use algorithms based on current equations of fault propagation to generate graphical simulations. The simulations are used to demonstrate a model of thrust propagation and thrust belt development that fits current knowledge of fault propagation. An alternative to the thrust transfer zone model is proposed, called thrust overlap zones.

The computer simulations provide useful information about the generation and behavior of multiple faults. The number of faults, the positions of their nucleation points and hence their density, the rock properties; and rate of fault propagation govern the uniformity of the shortening along the thrust belt. Thus, shortening of a thrust belt can be distributed more evenly by means of propagation of a large number of small faults than by a few large faults. The final geometry of a large thrust fault on a geological map provides few clues about its origin, i.e. whether it was produced by the coalescence of a series of en échelon thrust faults or from only a single fault. A simple kinematic model based on map length and position of known thrust faults imitates the curved fault map patterns of a segment of the thrust-fold belt of central Alberta.

INTRODUCTION

In the last two decades, the extensive mapping of thrust belts has greatly advanced the description and comprehension of thrust fault geometries. The deformation mechanisms leading to the horizontal shortening and vertical thickening of a thrust belt include: low-angle overthrust faulting, folding and layer-parallel shortening. The interference and overlap of the structures created by these mechanisms render it difficult to construct a kinematic model of the deformation leading to a particular set of structures. Hence, much remains to be done to understand the kinematics and deformation mechanisms that cause translation of large rock masses within thrust-and-fold systems.

The thrust fault mechanism has been extensively studied, particularly the linkage between individual thrusts in a thrust belt system, in attempts to explain why the shortening measured along a particular thrust belt remains relatively constant while individual faults have finite map length [or width, Fig. 1(a)] and varying displacements. Thrust transfer zones have been proposed as a common large-scale deformation mechanism for thrust-fold belts, particularly for examples from the Canadian Rocky Mountains (Douglas 1958a,b, Dahlstrom 1969). A thrust transfer zone is defined as the zone of overlap between two thrusts linked via a common underlying basal décollement. The observed succession of a series of thrusts with intervening overlap zones along the strike of a thrust belt led to the proposal that such thrust faults are correlative and delineate one or several linked thrust sets within the Rocky Mountain thrust belt (fig. 14 in Dahlstrom 1969). The transfer zone principle has since been used to explain the geometry of natural examples observed in thrust belts (Price & Mountjoy 1970, Brown & Spang 1978, Boyer & Elliott 1982, House & Gray 1982, Langenberg 1985, Tysdal 1986, Sanderson & Spratt 1992). It is used to explain why shortening apparently remains more or less constant across broad segments of thrust-fold belts, while individual faults have finite map lengths and show a progressive lateral decrease in their displacement.

However, the study of the final geometry of two neighboring faults or of a large segment of a thrust belt does not necessarily provide insight into the history of fault propagation, the timing of motion of the various faults relative to one another, and the sequence of thrust belt development. Several studies highlight the importance of the slow and progressive nature of the propagation of thrust faults (Elliott 1976a, Scholz *et al.* 1986, Walsh & Watterson 1988). The evolving nature of faults is critical to understanding the linkage between adjacent faults during the formation of a thrust belt. Furthermore, the sequential model of thrust faulting (i.e. hinterland-to-foreland fault development) is being challenged by theoretical models (Davis *et al.* 1983) and field studies (Boyer 1992). These models suggest a more complex history of faulting, where faults situated in the hinterland may be reactivated, while other faults situated near the toe of a deforming thrust wedge are being formed.

This paper attempts to clarify how thrusts propagate

*Present address: Institute of Sedimentary and Petroleum Geology, Geological Survey of Canada, 3303, 33rd Street NW, Calgary, Alberta, Canada, T2L 2A7.

and how varying amounts of displacement along individual thrust faults affect the geometry of a thrust-fold belt. A simplified geometrical model of thrust propagation for the cases of either a single or three branching thrust faults, showing the effects of thrust propagation on the geometry of a thrust belt, is presented. The model is developed within two computer programs, and illustrated with generated simulations of thrust faults.

The approach is similar to material analog models (clay cake or sandbox experiments) but it uses the computer to permit a quantitative correlation of the imposed deformation rate with naturally occurring geological phenomena, and to simulate the effects of a change in value of rheological variables on the shape of a fault or its rate of propagation in a rock sequence. So far few analog model experiments have been attempted to study the effects of lateral fault propagation on neighboring faults (Liu & Dixon 1991). The present programs attempt simulations of thrust faulting as seen in map view.

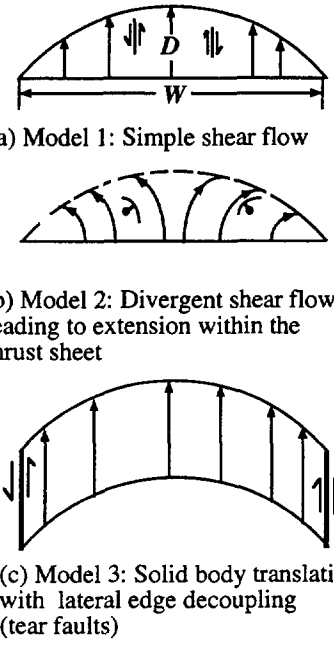

Fig. 1. (a)–(c) Comparison between various possibilities of simple models of kinematic patterns leading to a bow shape of a thrust fault in map view. These models neglect the effect of lateral thrust propagation. W is the thrust width, the maximum dimension of the fault plane measured perpendicular to the line of maximum displacement (D) of the thrust fault (see fig. 1 in Walsh & Watterson 1988). Here D is always considered to be in the center of W.

MODELS OF THRUST FAULT DEVELOPMENT

Three critical questions need to be addressed by models intended to portray the evolution of a series of thrust faults in a thrust belt: (1) the manner by which a single fault will evolve (fault propagation), (2) the deformation that will be caused by a single fault (displacement patterns in the hangingwall), and (3) the critical factors controlling a given rupture on a fault, in other words, specifically, why one fault will slip rather than another. By making some simplifying assumptions about the deformation, it is possible to model some aspects of the deformation of thrust belts. Where the nucleation and slip events of the faults are controlled, the first two questions are addressed, using the THREE THRUSTS computer program. The OVERLAP computer program addresses the third question and is presented later.

Thrust fault propagation and displacement patterns

Various models have been proposed to explain the kinematic evolution and/or the mechanics of a thrust sheet (e.g. Bielenstein 1969, Gretener 1972), but only recently has thrust fault propagation become the subject of debate. Older experimental models of thrust fault geometrical evolution used preexisting fault planes (Rich 1934), because these features were assumed to develop almost instantly at the beginning of fault motion. Douglas (1958a) proposed that thrust faults of the Rocky Mountain belt propagated gradually both laterally and towards the craton. Elliott (1976a) proposed that a thrust fault propagates radially from a point source, spreading sideways usually more rapidly than forward. The 'Bow and Arrow Rule' was derived from this relationship, which states that the maximum displacement of a thrust fault is a vector perpendicular to the center of the chord joining the thrust terminations in plane view. Elliott (1976a) also suggested that the value of this maximum displacement of a thrust fault was directly proportional to its map length. This hypothesis is now known to be a generalization of a more complex situation where all thrusts do not obey the rule, particularly because of variations in rock properties (Ellis & Dunlap 1988, Walsh & Watterson 1988, Cowie & Scholz 1992a,b, Gillespie *et al.* 1992).

Figure 1(a) shows a case of parallel displacement vectors of decreasing values from the center of the fault to its tips. This is a type of heterogeneous simple shear (Ramsay & Huber 1983) that can be accommodated in principle by a series of small faults or veins described by several workers (Price 1967, Harris & Milici 1977, Wojtal 1986, Lebel 1993). Gardner & Spang (1973), using experiments on clay cake models and predetermined fault locations and extensions, showed fanning effects in the hangingwall of a thrust from the middle of the fault (maximum displacement location) to its tip as the displacement along the fault decreased. A schematic portrayal of the divergent flow lines of such a fanning effect is shown on Fig. 1(b). From field observations, Coward & Potts (1983) showed a displacement gradient similar to that illustrated in Fig. 1(c) for a major thrust fault from the Moine thrust zone, where large shear zones or tear faults were found along the lateral sides of the thrust sheet. This case is clearly unusual in comparison to thrust-fold belts such as the Canadian Rocky Mountains where tear faults are relatively minor though important locally. Hence, several patterns of displacement flow lines can be visualized during the development of a simple thrust sheet, patterns which may be recognized through the study of the internal hangingwall defor-

mation (i.e. brittle or ductile deformation elements: mesoscopic or macroscopic faults, veins, shear zones, folds). The displacement pattern generated by heterogeneous simple shear (Fig. 1a) suggests internal strain spread more or less evenly throughout the thrust sheet (e.g. a series of vertical en échelon shear zones parallel with flow lines). Divergent flow lines (Fig. 1b) generate more extension along the leading edge of a thrust sheet compared to its hinterland portion (e.g. large extension veins vs. no extension) while solid body translation (Fig. 1c) should lead to few internal structures). In the light of studies of thrust sheets cited above, the heterogeneous simple shear model (Fig. 1a) appears to best explain internal mesostructures relationships.

Thrusts develop relatively slowly and incrementally, propagating through a rock body during an extended period of time (Elliott 1976a,b, Scholz *et al.* 1986, Walsh & Watterson 1988, Bombolakis 1992). One important aspect which is neglected by all the models illustrated in Fig. 1 is the effect of thrust propagation on the kinematic pattern of a thrust sheet. Recently, Liu & Dixon (1991) and Dixon & Liu (1992) were able to simulate thrust fault propagation using a centrifuge analogue model. Their results clearly show that significant layer perpendicular shear strain due to lateral fault propagation must contribute to the final state of a thrust belt. Laboratory and field data from micro- to macroscopic faults, show that displacement gradients measured along the length of faults often vary, but with an average gradient that tends toward a straight line (i.e. linear decrease in displacement, see Walsh & Watterson 1988, fig. 7 in Cowie & Scholz 1992a, fig. 16 in Dixon & Liu 1992), rather than an elliptical displacement curve as suggested by theories of elastic fracturing. Thus, it is reasonable to set up a numerical model of thrust growth that is based on a linear decrease of the displacement of the fault from its center to its lateral tip.

Another assumption of the model used herein is that the individual particles of material above the thrust fault are all transported parallel to the slip direction of the fault, along vertical planes, as portrayed in Fig. 1(a). Because of the various possible departures of natural strain patterns from this model, this simplified model cannot be applied to all cases of thrust sheet emplacement, but rather should be used as a basis for comparison. As shown below, this model enhances the comprehension of the effects of lateral thrust propagation and interaction of thrusts as thrust systems develop.

The spreading simple shear mechanism

Both numerical models presented here use the same deformation mechanism that is termed '*spreading simple shear*' in this paper. The spreading simple shear mechanism differs from ordinary simple shear since the width of the shear zone gradually increases as the thrust fault spreads laterally. Although the end product generated by the models might be relatively uniform shortening along the thrust belt, the driving mechanism is a series of translations of varying values, an adaptation of the heterogeneous simple shear mechanism presented in Fig. 1(a) (Fig. 2).

In the model presented here, the thrust sheet above a given thrust fault deforms through the spreading simple shear mechanism that permits both forward and lateral thrust propagation (Fig. 2). No folding or layer parallel shortening are allowed. While the center of the fault propagates forward and increases the displacement of the thrust sheet, the lateral tips of the fault propagate laterally. Immediately following the first event of lateral propagation of the thrust tips, the relative segments of the sheet left and right of the nucleation point (point F_0—Fig. 2a) are displaced by a series of vectors decreasing in value with a mirror-plane of symmetry from the center to both thrust tips. After each new increment of fault slip, the value of the total displacement relative to the footwall measured along the thrust trace is assumed to decrease linearly from the center of the fault (or initiation point) to the lateral tips (Fig. 2b).

The equations of Walsh & Watterson (1988) are used to translate the conceptual model into a workable mechanism. These equations express the relationship between the width of a fault (W), its maximum displacement (D, Fig. 1a) and its rate of propagation determined by rock properties. Thus, these equations permit derivation of a thrust fault propagation algorithm. Each fault nucleates from a predetermined point and evolves in a series of steps corresponding to slip events.

The suggestion of Elliott (1976a) that a linear relationship exists between maximum displacement and fault width for any thrust fault was contested by Scholz *et al.* (1986) and Walsh & Watterson (1988) on the basis of measurements of displacement made on faults observed in rocks of varying material properties. Rather, displacement appears to increase arithmetically relative to the fault width, with each successive slip event (Walsh & Watterson 1988) explaining the changing ratio of width to maximum displacement of natural faults.

Walsh & Watterson (1988) proposed an arithmetic growth model in which the relationship between fault width W (the maximum dimension of the fault plane measured perpendicular to the slip direction) and the maximum displacement D (usually found midway along the map length of a fault) on a single fault depends on material properties and is not linear but rather arithmetic (log–log), when the total number of discrete increments of displacement (slip events N) is large. Thus,

$$W^n = D \cdot P, \tag{1}$$

where P is a constant related to another constant k, both dependent upon rock properties (see equation A7 in Walsh & Watterson 1988) and $n = 2$ (see Cowie & Scholz 1992a, Gillespie *et al.* 1992 for discussion on the value of n, which may range between 1 and 2 but has little influence on the geometrical results presented here). We refer the reader to Walsh & Watterson (1988, equations A2, A5, A7) for a better understanding of the fault growth algorithms, definition of variables and relationship between k and P. Table 1 provides a summary of these equations. The relevant material properties are

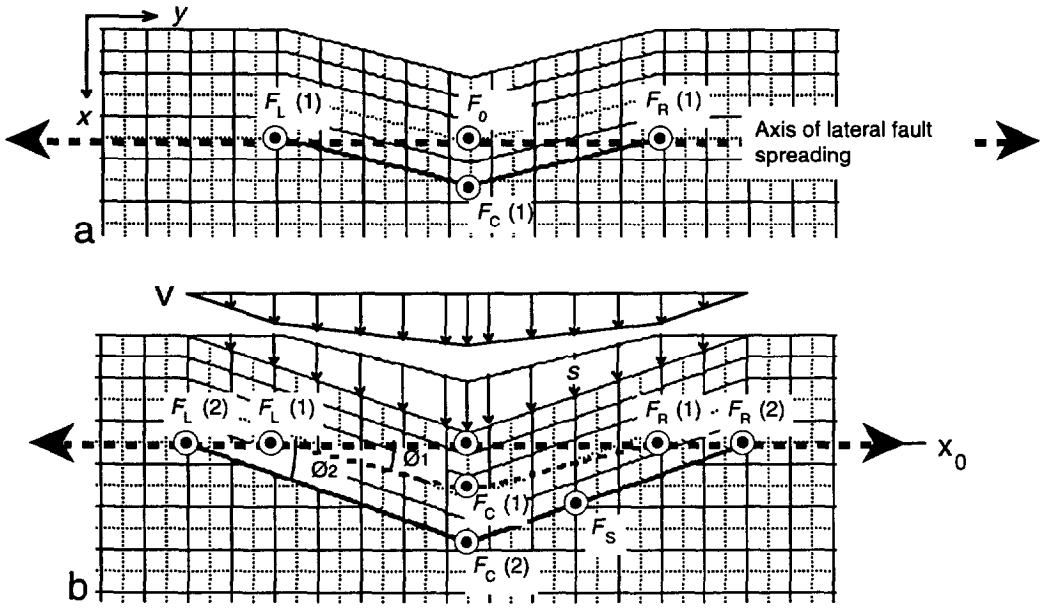

Fig. 2. The spreading simple shear deformation mechanism during thrust fault propagation. (a) Initial nucleation point and first fault slip increment. F_0 is the location of the fault nucleation point; $F_d(1)$ is the location of the frontal thrust tip after the first slip increment; $F_L(1)$ and $F_R(1)$ are locations of the left and right lateral thrust tips after the first increment. The axes of lateral fault spreading control the location of future left and right thrust tips. The calculated location of the frontal thrust tip and the location of the lateral thrust tips control the shape of the fault, and consequent hangingwall deformation. The first increment of fault slip applies two symmetrical simple shear deformations on the hangingwall of the thrust, dextral on the compartment left of F_0, sinistral on the right one. (b) The spreading simple shear mechanism controls each increment of fault slip. $F_L(1)$ and $F_R(1)$ are positions of fault lateral tips before slip increment (from $N = 1$ to $N = 2$); $F_L(2)$ and $F_R(2)$ are new positions of fault lateral tip; ϕ_1 and ϕ_2 are angles between the axis of lateral fault spreading and the frontal thrust center $F_c(N)$, before and after slip increment. Arrows in the upper part of the figure show the variation in value of the vectors of incremental slip. The rate of incremental deformation is higher between the old and the new lateral thrust tips because the fault is assumed to show a linear decrease in displacement from its frontal center point to its lateral tips. $F_S(N)$ is a point along the thrust frontal edge moving parallel to a shear plane S.

in decreasing order of significance: shear modulus, fracture toughness and friction on the fault surface (Walsh & Watterson 1988).

A seismic slip event u is the parameter usually used by earthquake seismologists to portray each increment of displacement on a fault. On a fault growing according to the arithmetic growth model, with last increment of displacement u_N (amount of slip in a slip event) and with N slip events, if successive events $u_1, u_2, u_3, \ldots u_N$ have a common difference, a, and the first term is zero

$$u_N = a \cdot (N - 1) \tag{2}$$

when N is small (see equation A1 in Walsh & Watterson 1988). The maximum and total displacement (D) measured in the center of the fault is the summation of all the increments of displacements u_N. In this model, a and k are fixed by the user so that each new value of $D(D')$ can be found easily:

$$D' = D + u_N. \tag{3}$$

See Appendix A and Fig. 2 for a description of the numerical model. Table 1 gives examples of values for a and k, as derived from the equations of Walsh & Watterson (1988), and their effect on the value of D for a fault of a specific width (W = 100 km). For a fixed value of a (case B1–B3, Table 1), the values of k and P must be greater to get faults with larger D. Since k influences the stress drop Δs at each slip event, only a certain range of values of k are possible to get realistic values of Δs (between 0.1 and 10 MPa for natural faults, Scholz 1990). For a fixed value of k (cases C1–C3), a must decrease to get large values of D. If a is too large, there are too few slip events N for a fault of a fixed D. A large range of values for k and a can still exist for faults such as those found in the Canadian Rocky Mountains thrust-fold belt where the shear modulus of the rocks G may vary between 3 and 30 GPa (see Gillepsie *et al.* 1992). It is beyond the scope of this paper to estimate the value of these variables, but it is helpful to know their possible range to understand the fault growth algorithm used herein.

COMPUTER PROGRAMS

The approach presented here uses a computerized adaptation of a clay cake or sandbox experiment where the computer is used to perform iterative operations to simulate a thrust belt being shortened; to do so, two different programs that run on an Apple Macintosh microcomputer have been developed to model two different aspects of the thrust belt kinematics:

(1) THREE THRUSTS simulates the deformation that one would observe in a thrust belt (or a sandbox) with infinitesimally thin thrust sheets propagating individually without being constrained by physical barriers.

(2) OVERLAP simulates a thrust belt using a deformation mechanism that permits an evenly distributed

Table 1. Examples of values of rock material constant k and slip increment a and variation of D for a fault with W = 100 km. Values in italics are preset, others are calculated. G: shear modulus; Δs: stress drop; μN: last (N) slip increment; N: total number of slip events. Equations derived from those of Walsh & Watterson (1988). Values calculated for different faults, F (A1–D3). Values for fault A1 are set and calculated according to the Lost River Fault, as described by Walsh & Watterson (1988). A value of G=10 GPa is assumed for rocks of the Rocky Mountains. B1 to B3 simulate a variation of k for a set value of a. Acceptable values for Δs range between 0.1 and 10 MPa, for intraplate earthquakes (Kanamori & Anderson 1975, Scholz 1990). C1 to C3 portray the result of varying the value of a upon a set value of k and Δs. D1 marks the values used for the simulation shown on Fig. 9. D2 and D3 shows more plausible values for the Rocky Mountains faults with D three times larger

F	D(km)	P	k	G(GPa)	Δs (MPa)	μN(m)	a (m)	N
A1	*5*	2000000	13888.9	*30*	2.9688	3.6	0.001296	2778
B1	*5*	2000000	13888.9	*10*	0.9896	3.6	*0.001296*	2778
B2	*10*	1000000	9820.93	*10*	1.3995	5.0912	*0.001296*	3928
B3	*50*	200000	4392.05	*10*	3.1294	11.384	*0.001296*	8784
C1	50.001	*199995.24*	*4392*	*10*	3.1294	11.384	*0.001296*	8784
C2	20.25	493815.4	*4392*	*10*	3.1294	11.384	*0.0032*	3558
C3	4.9847	2006125.1	*4392*	*10*	3.1294	11.384	*0.013*	876
D1	3.2488	3078030.4	*13870*	*10*	0.9909	3.6049	*0.002*	1803
D2	9.2824	1077310.6	*13870*	*10*	0.9909	3.6049	*0.0007*	5150
D3	9.2574	1080221.2	*4392*	*10*	3.1294	11.384	*0.007*	1626

$R = W/2$
$P = k2 \cdot 8 \cdot a$
$\Delta s = 1000\,(7 \cdot \pi \cdot G/16) \cdot u_N/R$
$D = W2/P$
$k = R/uN$
$uN = (2 \cdot a \cdot D)1/2$
$N = u_N/a$

shortening while numerous faults are allowed to nucleate and propagate.

The programs use the algorithms described in Appendix A and use the graphical output of the computer [a matrix of pixels (square dots), or bitmap] to keep track of the deformation, to impose incremental strain and to detect special situations. Bitmaps have been used in the past to simulate deformation of single objects or multiple objects within a homogeneous two-dimensional field (McEachran 1985—STRAIN GRAPHICS, De Paor 1987—STRAIN SAMPLER). The technique presented here differs in that the graphical objects (faults) direct the deformation via a series of predetermined growth algorithms. The graphical output is also checked so that the simulation obeys a set of empirical rules, which generates a graphic output that can be compared to geologic phenomena. Since these rules generate scale-dependent simulations, the simulation can represent faults of lateral extent at any scale ranging from several tens of meters to several hundreds of kilometers.

THREE THRUSTS program

In the program THREE THRUSTS, the computer screen is the device on which the evolution of the numerical model is followed. The computer screen view is an analog to what an observer would see if looking at the material surface in a sandbox, clay cake or centrifuge model, to simulate the evolution of a single or a series of thrust sheets. The model is set in a Cartesian (xy) reference frame, with the axis of shortening along the x direction (Fig. 2). The difference with respect to sandbox models resides in several boundary conditions described below.

Boundary conditions. In addition to assumptions regarding the spreading simple shear mechanism of thrust faulting as explained above, several simplifications have been introduced in the THREE THRUSTS computer model in order to generate simulations that can be easily understood and compared. These experiments may lead eventually to more complex models. The thrust sheets generated by the THREE THRUSTS model are assumed to be infinitesimally thin, so that no folds are generated either by ramping or movement above a décollement, and that the effects of thrusting can be isolated. No compensatory mechanism is used to maintain a uniform value of shortening along the thrust belt. In the model, having one thrust situated nearer the foreland than another one is taken into account so that the thrust positioned nearest the foreland deforms the hinterland ones when faults overlap (Fig. 3). The piggyback carriage of the hinterland thrusts by the foreland thrust imposes layer-perpendicular shear strains. Overriding of a foreland thrust by hinterland thrusts also needs to be properly simulated, since no assumptions are made about the sequence of thrusting and the individual thrusts are assumed to propagate synchronously. Hence, to get a simulation that has some relevance to the third dimension (or a $2\frac{1}{2}$ D simulation), a 'hinterland' thrust is allowed to mask a 'foreland' thrust as the former overrides a part of the latter. The imaginary material boundary surfaces of the model are defined in a manner similar to a sandbox model, with a hidden underlying plate, two opposite walls (the top and bottom of the computer screen, with the top wall converging towards the bottom), and the sides of the screen being modeled as free surfaces, as well as the surfaces between the observer and the computer screen.

Contrary to a real sandbox-centrifuge model, the

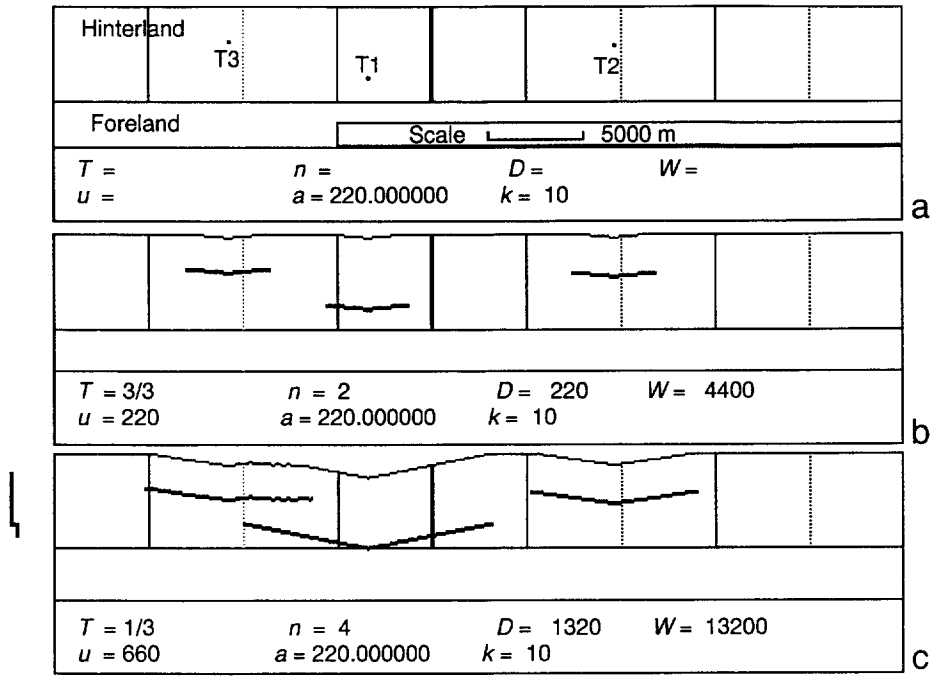

Fig. 3. Example of THREE THRUSTS simulation. (a) T1 to T3 are three thrusts ordered by their distance from the foreland. At the base of each display screen, T is the currently active thrust; a is the arithmetical growth factor (set by the user); k is the material properties constant (also set by the user); n is current number of slip events of T, and D is maximum displacement of T; W is total width of T, and u is current incremental slip. D, W, u and a are in meters. The thick vertical line represents the location of the schematic cross-section drawn on the extreme left. The simulations are scale-dependent. In all figures, the foreland is at the bottom.

mobile rear boundary is not modeled as a fixed rectilinear panel but as a surface that follows the movements permitted by the propagation of the thrust faults. Because we are using a model of a thrust belt where no mechanism of shortening other than thrust faulting is allowed (i.e. no folding or layer-parallel shortening), and because only a few active faults are present, the shortening along the belt is not evenly distributed until substantial overlapping of the faults occurs. This mobile rear boundary is used to observe the effect of thrust propagation on predetermined structures. Another simple rule does not allow a foreland thrust to cut through an overlying, hinterland thrust but only to merge with it. This eliminates the possibility of out-of-sequence faults cross-cutting and demobilizing earlier thrusts. Appendix B gives more details about the operation of the THREE THRUST program. Figures 3–5 and Appendix B describe the basic operation and special situations.

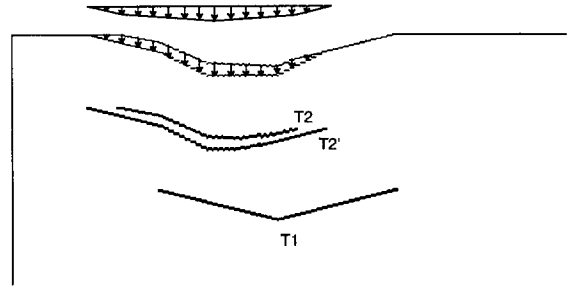

Fig. 4. Example of vectorial addition of the incremental displacement on a non-rectilinear thrust. After being subject to asymmetrical layer-perpendicular shear strain by T1, T2 has been deformed (initial state of T2 not shown). From its new position, T2 advances to T2′ through spreading simple shear. The distribution of the incremental displacement in the hangingwall of T2′ (shown by the displacement vectors in the upper part of the figure) conforms to the spreading simple shear mechanism and is identical to the one of a rectilinear thrust (see Fig. 2).

Thrust simulations. Several interesting phenomena, important for understanding thrust belt evolution, can be observed using the THREE THRUSTS program. Simplifications are inherent to the computer model and observed features within the simulations can be correlated with natural examples.

(1) *Superimposed shear strain due to piggyback thrusting*. Hangingwall strain during thrust propagation is an important kinematic mechanism. During the development of a thrust belt, a rock body may go through a series of deformations related to the propagation and advance of lower thrust faults transporting it in a piggyback manner. Some of the more important strains will be caused by shear strain within the thrust sheet, termed 'piggyback strain'. For example, in Fig. 6(a), the right side of the T2 thrust sheet undergoes sinistral simple shear during an episode of thrust propagation and advancement, but this simple shear strain is overprinted by the dextral simple shear introduced by the propagation of the left side of T1 (Figs. 6b & c), a thrust fault closer to the foreland that overlaps part of T2.

Situations involving several thrust faults propagating within a common time span would create complex kinematics and incremental strain histories in individual thrust sheets. Field observations in thrust sheets of the Front Ranges of the Canadian Rocky Mountains (Lebel

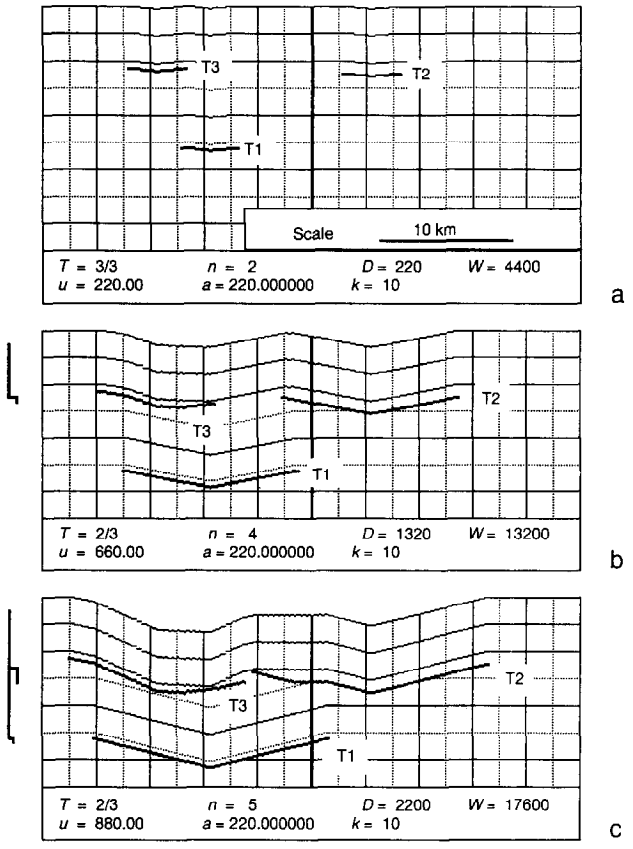

Fig. 5. Special geometric case where one tip of a hinterland thrust (T3) propagates in front of one tip of a foreland thrust. Three thrusts initially ranked T1 to T3 using their positions relative to the foreland in (a) propagate to new positions in (b). After incremental layer-perpendicular shear strain by T1 on T3, T2's left lateral tip becomes situated in a more hinterland position than T3's right lateral tip (b). Eventually, after additional lateral propagation from its position in (c), T3 will become a footwall fault of T2. In turn, the left part of T2 will be carried piggyback by both T1 and T3. In a natural setting, this phenomenon is a geometrical necessity but in the case of a computer simulation, a particular algorithm in the program needs to handle the geometric switch between T2 and T3 so that T3 does not cut through T2 while propagating. Rather, T3 will continue to propagate underneath T2 and merge with T2 to form a duplex where T2 will be carried piggyback.

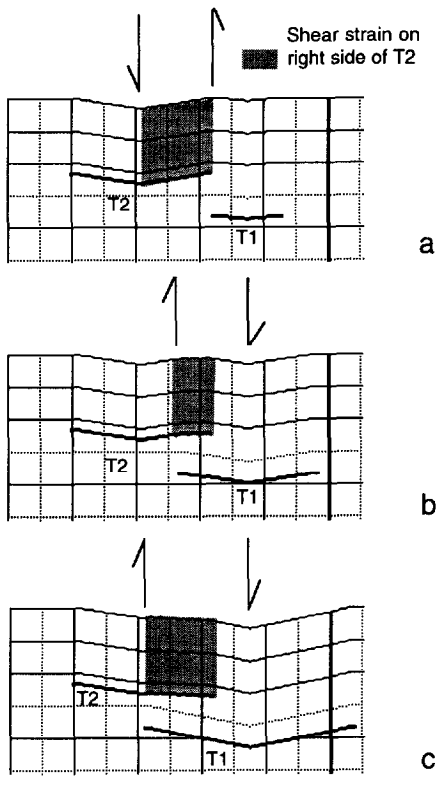

Fig. 6. Reversal of shear strain induced by two propagating thrust faults. After sinistral simple shear in the right part of the hangingwall of T2 induced by thrust propagation and motion, the propagation of T1 leads to a dextral simple shear in the same area, although the final strain pattern of T2's thrust sheet might lead one to conclude that no layer-perpendicular shear deformation has occurred.

1993) show subvertical shear zones, sub-perpendicular to regional thrust faults, with opposite shear sense, cross-cutting each other in a seemingly simple regional tectonic context. Such structures may have been overlooked in the past or mistaken as evidence for two or more phases of deformation. Clearly, hinterland thrust sheets should have undergone a longer-lasting and more complex strain history of shear than foreland sheets.

(2) *Kinematic interpretation of thrust branch points*. The line of intersection of two fault planes is termed a branch line; the point of intersection of the branch line on the topographic surface or the point of intersection of two thrust traces on a geological map is termed a branch point (Boyer & Elliott 1982, Hossack 1983). Branch lines can originate in different manners in nature, which has important implications for computer simulations in as much as thrust branch points are in fact the more difficult aspect of thrust propagation to model numerically. The meaning of thrust branch points in nature or as projected on geological maps can be uncertain and several interpretations can be given, depending on what we know about the relative position of each fault (Boyer & Elliott 1982, Diegel 1986).

In simulations of two neighboring nucleation points situated close to the same y axis, a variety of different types of branch points and thrust sheet behaviors are observed depending on relative initial positions along the x axis and the sequence of thrusting. For two thrust (T1 and T2) nucleation points, three sequences of thrusting can be simulated: (1) T2 formed before T1 (Fig. 7a), (2) T1 formed first (Fig. 7b), and (3) the two faults propagated synchronously (Fig. 7c).

In case 1 (Fig. 7a), where T2 propagates first, the center part of T2 advances ahead of the lateral propagation axis of T1 and stops. The lateral propagation of T1 then leads to a branch point where the right part of T1 continues to propagate under T2 to form a duplex. T1 and T2 will then tend to become parallel as T1 continues to propagate (Fig. 7a3). The branch point will not move laterally during further propagation of T1 under T2.

Case 2 (Fig. 7b), where T1 propagates first, leads to imbrication of T1 by T2. T1 overlaps the nucleation point of T2, and T2 is carried ahead of the right lateral tip of T1 (Fig. 7b1). Then, motion on T2 will lead to an initial branch point along the right leading edge of T1 (Point X, Fig. 7b2). Since T2 and T1 are at a high angle to each other and emanate from the same décollement, T2 will gradually advance over T1 and carry material

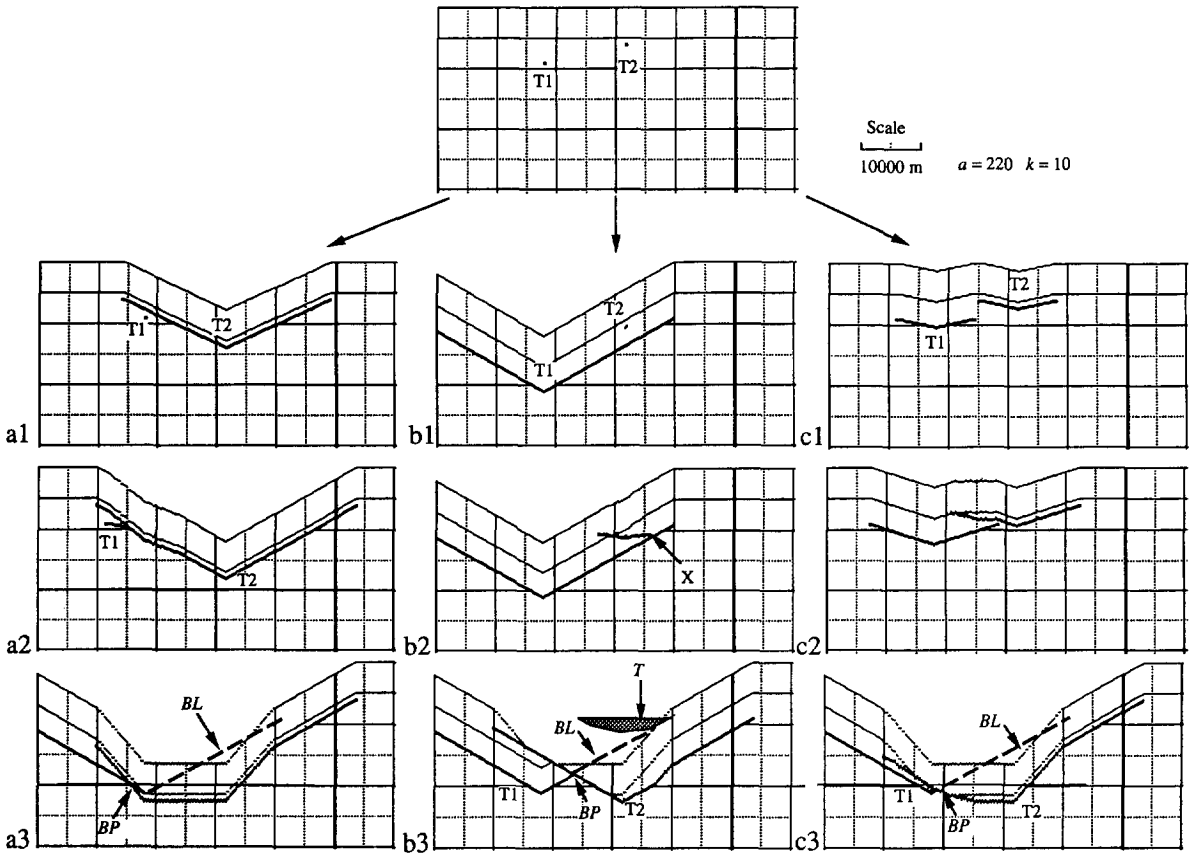

Fig. 7. Comparison of the influence of the sequence of thrusting on the final geometry of a thrust zone. Three sequences of thrusting are represented, each starting with identical locations for the nucleation points of thrusts T1 and T2, slip parameters and scale, and ending with equal numbers of slip events for each fault ($N = 11$). The sequence in (a) represents a case with the hinterland thrust T2 reaching its full width before T1 starts to form. The sequence in (b) shows the opposite case. Point X on (b2) shows the location of the initial branch point between T2 and T1. The sequence in (c) represents a case of synchronous thrusting where T1 and T2 slip alternatively until $N = 11$. The geometries of the simulated thrust belts at the end are sharply different although equivalent shortening distributions are observed for the three cases at the back of each thrust belt [top of each graph, (a3), (b3) and (c3)]. BP, branch point between the two thrusts; BL, branch line; T (shaded area), torn part of T1 by the propagation of T2.

that used to be part of T1 to the right of the initial branch point between T2 and T1 (Fig. 7b2). The initial location of the material that was part of T1 and transported as a part of the leading edge of T2 at the end of the simulation is shaded (T) in Fig. 7(b3).

In case 3 (Fig. 7c), thrusts T1 and T2 propagate with alternating slip events. In the simulation, the branch line moves gradually backwards relative to T2 and the branch point moves towards the center of T1 as the deformation progresses. Such displacement of the branch line may be represented in the field by wide shear zones between natural faults close to the branch point.

Thus, computer simulations predict different branch line geometries and hangingwall shear strain for varying sequences of thrusting.

(3) *Kinematic model of a large segment of a thrust belt.* A numerical simulation of thrust faulting involving hangingwall deformation becomes increasingly difficult to handle as the number of faults involved increases. However, here the use of visual markers on the computer screen simplifies calculations. A sequential model of thrust belt evolution is made on the computer screen by successively pasting in the result of incremental deformations along individual faults. Here, the model is used to simulate the evolution and approximate a kinematic model of the Front Ranges and Foothills of the Canadian Rocky Mountains between the Athabasca and North Saskatchewan rivers (Figs. 8 and 9). The construction of the model is straightforward and leads to a close approximation of the present pattern of thrust faults in this area (compare Figs. 8 and 9e).

The generation of a large thrust fault ($W > 50$ km) using approximate but realistic a and k values (see Table 1) needs a substantial number of slip events ($N > 1000$). Thus it was chosen in this case to work with a sequential model where only one fault was active at a time, to shorten simulation time. A particular fault is generated by measuring its map length, an approximation of W (see Gillepsie *et al.* 1992 for discussion), and letting the program run until this value is reached. To deform the area with a new fault, the computer screen output is 'copied' (captured) and 'pasted' into a new simulation.

To construct the series of simulations shown on Fig. 9, values of a (0.002) and k (13,870) were kept constant for all faults and were set to approximate rock properties of sequences in the Canadian Rocky Mountain Front Ranges and Foothills (which consist mainly of clastic and carbonate sedimentary rocks, Table 1). The projection was set to 1:1,000,000, to image effects of large thrust

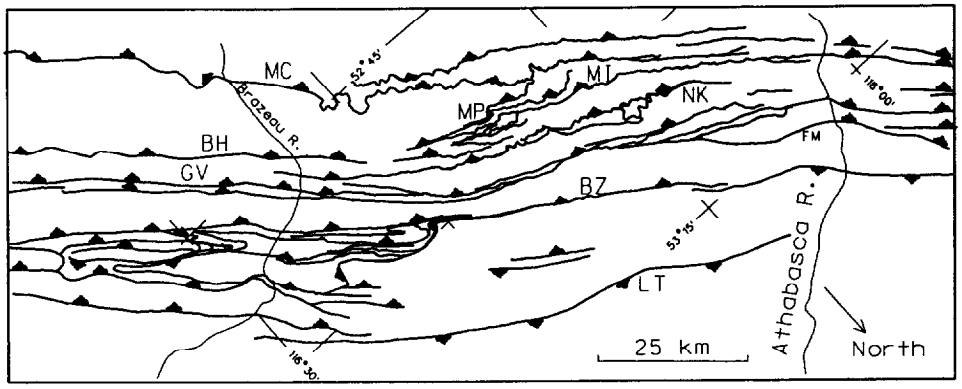

Fig. 8. Map of the thrust faults observed in the Canadian Rocky Mountains and Foothills in the Athabasca–Brazeau region. Thrust faults: Bighorn (BH), Brazeau (BZ), Folding Mountain (FM), Grave Flats (GV), Lovett (LT), McConnell (MC), Miette (MI), Mountain Park set (MP), Nikanassin (NK). Compiled from Mountjoy (1960b), Price *et al.* (1977), Mountjoy *et al.* (1992), and Douglas & Lebel (1993).

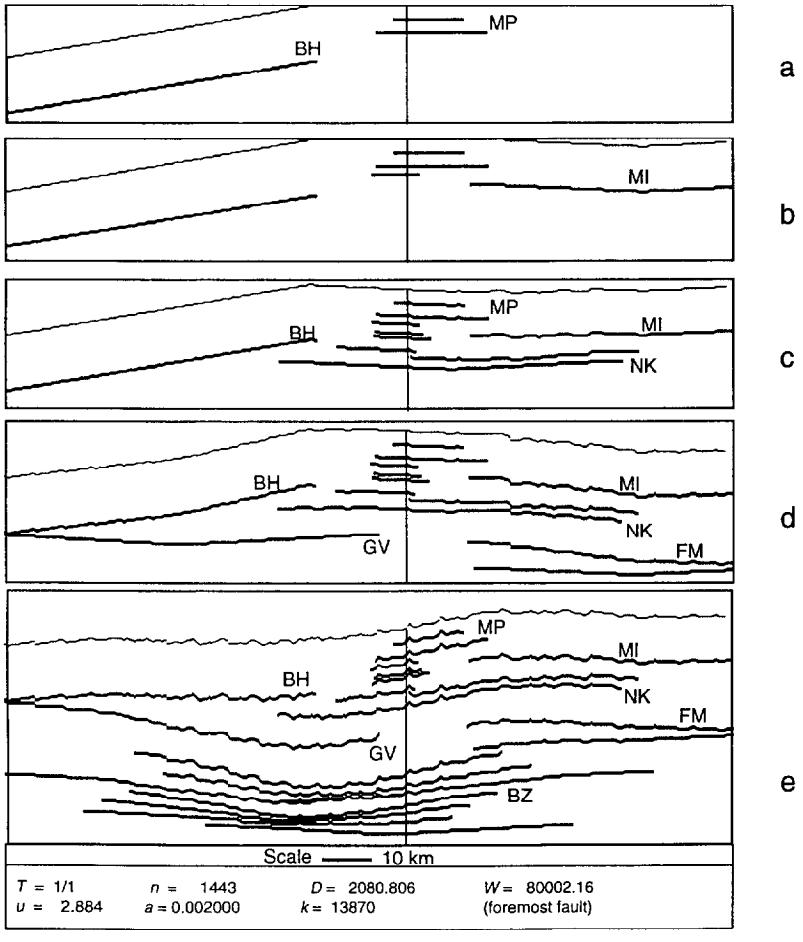

Fig. 9. THREE THRUST simulation leading to an approximation of the map pattern observed on Fig. 8. See text for explanation. Refer to Fig. 8 for thrust labels.

faults. At this scale, with the chosen a and k values, short faults ($W < 33$ km) do not have any effect on the simulation, because their maximum displacement is smaller than 353 m (1 pixel) and do not reach the critical value of 1 pixel for minimum translation within the bitmap. The small faults shown in the simulation have only been set as markers to follow the deformation (e.g. some of the numerous faults located near Mountain Park—Figs. 8 and 9b&c). The width of each modeled fault was first measured on geological maps of the area (Mountjoy 1960a,b, Price *et al.* 1977, Mountjoy *et al.* 1992, Douglas & Lebel 1993), then the progression of the deformation involving the formation of each new fault was modeled. Only one fault was active at a time. The faults were activated so that the first faults occurred in the hinterland and the last ones in the foreland following a classical foreland-directed progression of deformation. Reference lines in upper part of Fig. 9(a) and subsequent drawings show the total shortening accomplished along each new fault.

The end-product (Fig. 9e) is not a realistic image of the deformation but is a quantitative simulation. The

displaced reference line in the top part of Fig. 9(e) has a final shape comparable to the McConnell thrust (MC). It shows, as do other faults in the foreland [like the Nikanassin (NK), and other thrusts behind to the southwest] a sigmoidal shape related to the sinistral shear resulting from the consecutive development of the numerous faults representing the Brazeau structure (Sanderson 1939, Hake *et al.* 1942, MacKay 1940a,b, Douglas 1958b, Douglas & Lebel 1993). Most faults exhibit this sigmoidal shape on the geological map (Fig. 8). Thus, the simulation provides a kinematically plausible explanation for the final general shape of the different faults. A few faults like the Grave Flat thrust (GV) have a shape and orientation considerably different from the one generated by the simulation in the above model. However, if the fault is out of sequence, as suspected by the construction of a balanced cross-section of that area (Douglas & Lebel 1993, Lebel 1993), it would explain the lack of correlation with the computer simulation.

Another benefit of the above approach is to test whether the a and k variables used in the simulation have realistic values. A comparison of the end-product with the geological map shows that the mapped degree of curvature of the various faults described above is generally higher than what has been generated by the model. This can be explained in several ways: (1) several faults have not been included in the simulation because they were not large enough to model, (2) folding was not taken into account, (3) the slip parameters are not valid, suggesting that different values should be used to permit more displacement to be attained for a certain width of a fault, (4) the thicknesses of the thrust sheets are not considered, and (5) the simulation represents faults which are not subject to erosion. Together, these points explain the discrepancy in fault curvature. Another discrepancy is the total shortening in the simulation compared to that measured from the Cretaceous Cadomin Formation, within the Foothills thrust belt. It is estimated to be about 35 km on a cross-section close to the Brazeau River, as measured between the McConnell thrust fault trace and the triangle zone Lovett backthrust fault (Douglas & Lebel 1993, Lebel 1993). This value is three times the shortening measured on our simulation for the same area. Because points 1, 2, 4 and 5 cannot account for this discrepancy, it is thus clear that the slip values of these faults are not correct and should be changed for more appropriate values. One approach is to decrease the slip value a by a factor of 3 (to 0.7 mm), which would give roughly a value of D three times larger for an identical large thrust but with a substantially larger number of slip events N (see Table 1, D2). Another solution is to increase a to 7 mm and decrease k (to 4392; D2 in Table 1) roughly three times for an equivalent value of N. Only a better constraint on the duration of the construction of the thrust belt and an idea of the strain rate may help to ascertain which of several solutions is the more realistic.

(4) *Multiple-fault origin of major thrusts.* Ellis & Dunlop (1988) suggested that a major thrust can be made up of a series of coplanar smaller faults, which merge at certain points to form a larger fault, and suggested that some fault bends can be interpreted to be merging points (see also discussion and fig. 16b in Dixon & Liu 1992).

Figures 10(a)–(c) provide a computer simulation of how three en échelon thrust faults from a common décollement (Fig. 10a) can lead to a simple displacement gradient at the back of the thrust belt (Fig. 10c) similar to that of a different simulation for only a single thrust fault (Fig. 10d). There is no obvious difference in the final configuration of the thrust trace and shortening gradient for both simulations. The case presented in Figs. 10(a)–(c) uses a synchronous thrust sequence like that illustrated on Fig. 7(c). The right lateral tips of T2 and T3 stopped just short of the leading edge of thrust T1 at the end of the deformation, so that no fault propagated laterally to the right leading edge of the footwall thrust like in the case illustrated on Fig. 7(b). Because the three thrusts are stacked one on top of each other, they give the impression that they are a single fault, with only some small imbrications branching away from the main thrust. Such fault trace geometry is common on geological maps and there is no clear way to distinguish between a single and a multiple fault origin of the hangingwall strain. Thus, when reconstructing a large thrust belt using the final width of thrust faults as shown above (Fig. 9), it must be kept in mind that some of the larger thrust faults might in fact be an assemblage of several or many smaller faults.

The overlap mechanism

A simplified model of thrust belt development, the 'overlap mechanism', can be used to explain the relatively uniform shortening that occurs in different segments of thrust-fold belts. As shown in the preceding sections, the lateral propagation of each individual thrust fault along a thrust belt gradually leads to the overlap of some of the faults. The piggyback layer-perpendicular shear that is induced by individual thrust faults on other thrust sheets is the first part of the composite mechanism leading to a relatively uniform shortening in a thrust belt. The second part of this composite mechanism is the 'overlap mechanism'. It explains how thrusts in a thrust belt can be viewed as an evolving system, where a network of propagating thrust faults exists at all times, but only the faults situated in the best position to accommodate shortening will slip and thus propagate even farther laterally.

Studies of present-day active thrust faults in New Zealand and California show that they propagate by means of local stress buildup, due to the inhomogenous shortening along the thrust belt, and the eventual stress release through fault slip (Schwartz & Coopersmith 1984, Berryman & Beanland 1991). Hence, in an area with a series of faults that overlap each other in map view, the fault which is situated in the most critical position will slip and propagate farther laterally and towards the foreland. If there is no fault placed in this critically strained area, a new fault will nucleate. This

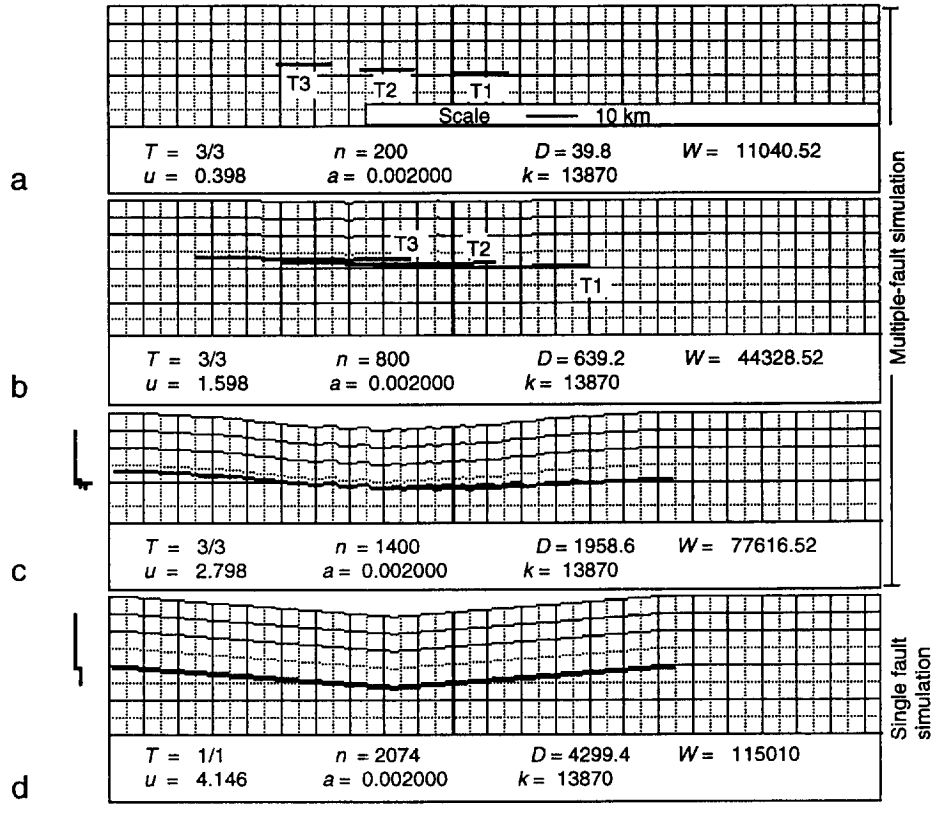

Fig. 10. Example of two different simulations leading to a similar configuration of a thrust fault, using realistic a and k values. The first simulation (a)–(c) shows three faults which after nucleation and initial propagation (a), start to overlap each other, where the more foreland ones carry the others piggyback (b). The piggyback strain on the hangingwall thrust faults eventually leads to their propagation toward and against the leading edge of the lowest thrust (c) and the consequent fault coalescence. The second simulation (d) generated with only one active fault leads to almost the same final strain pattern as (c). The lines drawn on the left are schematic cross-sections along the thick line near the center of the diagram. The lines on the cross-sections represent the relative fault length of each thrust from its initial breaking point to its leading edge.

switching of slip between one fault and another in a series of overlapping thrust faults is herein termed the overlap mechanism. A simplified computer model, the OVERLAP program, demonstrates the applicability of this concept and mechanism.

OVERLAP program. The OVERLAP computer program was written as an attempt to show how a series of thrusts propagate laterally and overlap each other, allowing one to observe the structural evolution and continuous uniform shortening of a thrust belt. It was conceived as a complement to the THREE THRUSTS computer program which does not illustrate the overlap mechanism. Several simplifications have been made to formulate a working model.

Boundary conditions and description of the overlap mechanism. OVERLAP, in contrast to THREE THRUSTS, allows up to 50 thrust faults to nucleate and propagate within a thrust belt spanning 400 pixels in width and 50 pixels in length (Fig. 11). However, the visual aspect of the model is similar to THREE THRUSTS and the algorithms used to control thrust propagation (values of D and W) are the same as in the THREE THRUSTS program, so that the user can change a and k. OVERLAP does not permit the deformation of the hangingwall of each fault because of the increasing complexity of handling fault intersections and longitudinal deformation as deformation proceeds (as demonstrated by THREE THRUSTS). Instead, OVERLAP uses a histogram in the middle part of the computer screen, that shows the amount of shortening at the rear of the thrust belt, evaluated in pixels (Fig. 11). The shortening resulting from the motion of the different faults after each slip event can be observed continuously. The maximum value of 50 faults may appear high but it was chosen to see if the parameters set by the user tend to generate a large number of faults, or if only a few are necessary to achieve the desired shortening along the thrust belt.

In the computer model, the overlap mechanism is conceived as follows. The different values of shortening found along each pixel column and represented on the histogram are used to search for the minimum value which then becomes the most favored pixel column for future thrust movement. If a series of contiguous minimum and equal values are found, the program chooses the one situated midway between the next higher values of shortening. When the minimum value of shortening is found, the program looks for a thrust which overlaps the related pixel column. If there is one, the fault is allowed to move an additional slip event and propagate laterally to an extent governed by the equations of Walsh & Watterson (1988). The shortening value of each pixel

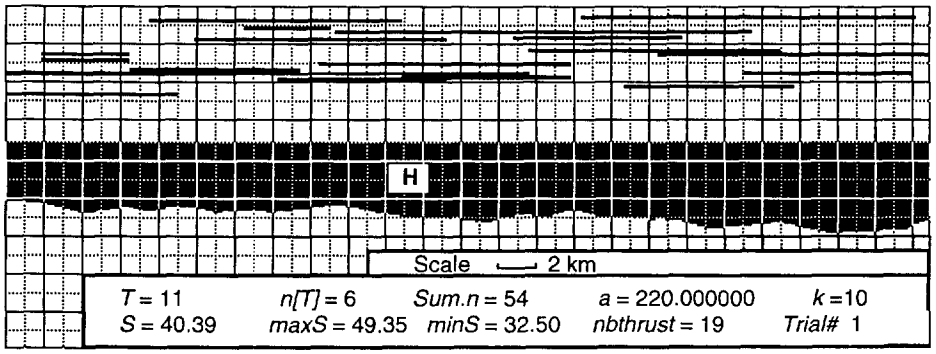

Fig. 11. Example of OVERLAP simulation. The program generates new faults where the shortening is a minimum if no other faults are close enough to permit any shortening. The shortening accommodated by the various faults situated in the upper part of the diagram is represented in the middle part of the diagram by a downward facing histogram (H) of the cumulative displacement of all overlapping faults. T: current active thrust number; $n[T]$: number of slip events that T has undergone; *Sum. n*: sum of all n that occurred within the simulation; a and k:, slip and mechanical properties variables (Walsh & Watterson 1988); S, *maxS* and *minS*: average, maximum and minimum value of shortening in pixels (1 square = 1000 m); *nbthrust*: number of thrusts within the belt.

column is incremented by adding the values calculated using the spreading simple-shear mechanism (identical to the one used by the THREE THRUSTS program). The computer program then loops and proceeds to find a new minimum value of shortening. If no fault is found overlapping the minimum shortening pixel column, the program then proceeds to create a new nucleation point on the minimum pixel column and allows its first slip increment. The location of this nucleation point along the pixel column is chosen randomly.

If the number of thrusts reaches the arbitrary value of 50, the OVERLAP program will no longer generate new nucleation points but rather looks for the closest thrust fault in the event that none overlap the minimum pixel column. In order to limit the number of new faults and to allow for the simulation of a certain stress buildup before a new fault will nucleate, new thrusts are only generated if the minimum value of shortening is lower than half the average shortening of the entire thrust belt. The program stops when the arbitrary value of 50 pixels (5 km) of average shortening is reached over the width of the thrust belt.

Experimental results. The overlap mechanism described above provides a good model for transforming the strain applied by a backstop within an imaginary sandbox into relatively uniform shortening in an algorithmically growing thrust belt. All the test runs performed with this model showed a relatively uniformly distributed shortening (with local minor variations). The highest variations in shortening (between 40% and 60% relative to an average shortening of 50%) were observed in thrust belt simulations using high propagation rates. Several tests were run to determine the importance of the rheological and slip factors on the final number of faults. These experiments showed a number of interesting features:

(1) The number of faults needed for 50% shortening depends upon the rate of lateral fault propagation. If the faults propagate slowly, as in hard rock (e.g. $a = 0.002$, $k = 10{,}000$), the number of thrusts needed is high and rapidly reaches the maximum allowed number of faults. In contrast, only 15 faults accommodate the same shortening uniformly if propagating at an unrealistically fast pace (less than 60 slip events for $a = 220$ m, $k = 10$).

(2) Abnormal results are produced particularly in the initial stages. When using slip and rheological values comparable to natural cases ($a = 0.002$ m, $k = 13{,}870$), the faults are very slow to propagate and the computer program rapidly initiates the largest number of possible faults, but not uniformly, the faults being concentrated in the left part of the computer screen because the program scans for minimum values of shortening from left to right. To prevent abnormal thrust concentrations, and to allow uniform shortening within the thrust belt simulation, the computer program permits 50 random nucleation or weakness points to be generated initially.

(3) The locations of the nucleation points of faults along the thrust belt are important because the area with the highest concentration of faults tends to show shorter individual fault lengths (Fig. 11). This means that fault propagation is less favored in areas which have a high density of faults. Random nucleation permits comparison of different possible natural cases where weakness points may or may not be concentrated in certain areas.

DISCUSSION

The transfer zone mechanism (Dahlstrom 1969, 1970) vs. the overlap mechanism

The thrust transfer zone mechanism of Dahlstrom (1969, 1970) has been used to explain the phenomenon that although displacement on individual faults varies significantly along strike, the net displacement across the whole thrust belt remains approximately the same when measured from one cross-section to another. To explain this uniform shortening within thrust-fold belts, Dahlstrom suggested that along the extreme lateral parts of individual thrusts, zones of exchange of displacement (transfer zones) occur with en échelon, overlapping thrusts. Dahlstrom (1970) explained that the basal décollement was the mechanism linking the

thrusts, and this remains valid. However, it is implicit in this concept that thrusts were believed to show a decrease in their displacement mostly in the portions overlapping other thrusts. In addition, paired en échelon faults within transfer zones are assumed to have grown simultaneously (Dahlstrom 1970, p. 358).

In light of current knowledge about thrust fault propagation, the thrust transfer zone model is problematic, because it is difficult to explain how two faults that are now neighboring and en échelon, and are assumed to have had a long history of lateral thrust propagation, could have transferred their displacements when the nucleation points of the faults were several hundreds of kilometers apart. For example, the current positions of the Miette and McConnell thrust faults (Fig. 8) suggest that they were linked by a transfer zone (fig. 14 in Dahlstrom 1969). The probable nucleation points of these thrusts are centered between the lateral tips of the respective faults (Miette, near the Athabasca River, McConnell near the Red Deer River) approximately 300 km apart. Thus, the overlap of the two faults should be envisioned as the consequence of gradual lateral propagation, with the two faults overlapping in the later stages of their development, if each fault is also assumed to evolve from a single fault or point.

Our modeling suggests that it is doubtful that the thrust belt would have developed without other overlapping faults being generated to take up compression in the area between the early McConnell and Miette faults. For shortening to be evenly distributed along the thrust belt, it is clear from the OVERLAP computer simulations that many thrusts should be active during the evolution of the belt, some of the more hinterland thrusts being reactivated while foreland thrusts are being formed. Current knowledge about thrust fault activation also shows that all parts of each thrust are not necessarily active during each slip increment as in the model presented here. Future work should consider the cause of these variations and attempt to construct a better model of thrust propagation considering this aspect.

Simulations presented here suggest that during the development of a thrust belt, the displacement is not transferred or exchanged between pairs of faults, rather it is an individual fault that is initiated and propagated through fault slippage when a sufficient stress occurs. Thus, overlap of two or more faults should be envisioned as the consequence of thrusts propagating throughout the thrust belt, rather than a special mechanism that links two or a few individual faults. In light of this, zones of thrust overlap should be termed 'overlap zones' and the misleading term 'transfer zones' abandoned.

Other controls on thrust fault propagation

As noted above, the initial location of the fault nucleation point and the propagation rate of the various faults in the active thrust zone will affect the geometry of the thrust belt. Other factors such as pore pressure, thickness and taper of the orogenic wedge are important and are well described by the critically tapered Coulomb wedge model presented by Chapple (1978), Davis *et al.* (1983), Dahlen *et al.* (1984) and Dahlen (1984). Future modeling should consider these variables to improve the realism and comparative validity of the overlap mechanism. For instance, if a rock package with finite thickness could be simulated, the foreland propagation of thrust faults induced by an increase in taper could be modeled (Dahlen *et al.* 1984). This type of model should account for ramping through a thick rock package, the formation of folds and the eventual layer-perpendicular shear of various thrust sheets through stacking and piggyback transport of thrust sheets as observed in natural examples.

CONCLUSIONS

Two computer programs with graphical simulations demonstrate a model of thrust propagation and thrust belt development based on current knowledge about fault propagation. This new model is a composite of two mechanisms:

(1) The spreading simple shear mechanism applies a form of layer perpendicular simple shear strain symmetrical about the center of the leading edge of a thrust fault to its lateral tips, as the fault propagates laterally and forward.

(2) The overlap mechanism is a conceptual model derived from computer simulations and thrust fault theory that predicts when each fault might propagate when a group of thrust faults are linked through a common décollement. The mechanism is an analog of local stress buildup and its eventual relaxation by slip on a full best-situated to accommodate this stress release.

The OVERLAP program shows that thrust faults propagate laterally and do not transfer displacement from one thrust to another; variations in displacements along strike are the consequence of multiple thrust initiation sites. Thus, a composite mechanism of the overlap and spreading simple shear mechanisms provides a better way of visualizing the evolution of thrust belts than the thrust transfer zone concept of Dahlstrom (1969, 1970).

The computer simulations provide useful information about the behavior of multiple faults:

(1) The number of faults and the location of their nucleation points (their density), and the rock properties and consequent rate of fault propagation relative to the rate of shortening govern the uniformity of the shortening along the thrust belt.

(2) The branch lines and hangingwall strain pattern of two intersecting thrust faults can be used to unravel the sequence of thrusting of the two faults.

(3) The OVERLAP computer simulations show that shortening along a thrust belt can be distributed more evenly by means of propagation of a large number of small faults than by a few large thrusts.

(4) The THREE THRUSTS computer simulations

also demonstrate that the final geometry of a large thrust fault on a geological map leaves few clues about its origin, whether it was produced by the coalescence of multiple, en échelon, thrust faults or from only a single fault.

TECHNICAL INFORMATION

The programs were written in the V.I.P. language (Visual Interactive Programming, Copyright 1986, 1987 by Mainstay) and run on a Macintosh microcomputer. They are available from D. Lebel as compiled or ASCII files. To obtain a copy please send $25.Cnd for duplication and handling costs.

Acknowledgements—The paper is part of a Ph.D. thesis by D. Lebel which was supported by the Geological Survey of Canada (1986–1988), Québec FCAR scholarships (1985–1987) and the Geology Graduate Scholarship of the Canadian Society of Petroleum Geologists (1986). We acknowledge stimulating discussions with Andrew Hynes in the early stages of this research project and the very helpful comments of Raymond Price, Deborah Spratt and Glen Stockmal. We also appreciate the comments from Deborah Spratt as a journal reviewer, an anonymous person and from Steven Wojtal, associate editor of *J. Struct. Geol.*

REFERENCES

Berryman, K. & Beanland, S. 1991. Variation in fault behavior in different tectonic provinces of New Zealand. *J. Struct. Geol.* **13**, 177–189.

Bielenstein, H. U. 1969. The Rundle thrust sheet, Banff, Alberta. Unpublished Ph.D. thesis, Queen's University, Kingston, Ontario.

Bombolakis, E. G. 1992. A development stage of a foreland thrust belt. In: *Thrust Tectonics* (edited by McClay, K. R.). Chapman & Hall, London, U.K., 33–40.

Boyer, S. E. 1992. Geometric evidence for synchronous thrusting in the southern Alberta and northwest Montana thrust belt. In: *Thrust Tectonics* (edited by McClay, K. R.). Chapman & Hall, London, U.K., 377–390.

Boyer, S. E. & Elliott, D. 1982. Thrust systems. *Bull. Am. Ass. Petrol. Geol.* **66**, 1196–1230.

Brown, S. P. & Spang, J. H. 1978. Geometry and mechanical relationship of folds to thrust fault propagation using a minor thrust in the Front Ranges of the Canadian Rocky Mountains. *Bull. Can. Petrol. Geol.* **26**, 551–571.

Chapple, W. M. 1978. Mechanics of thin-skinned fold-and-thrust belts. *Bull. geol. Soc. Am.* **89**, 1189–1198.

Coward, M. P. & Potts, G. J. 1983. Complex strain patterns at the frontal and lateral tips to shear zones and thrust zones. *J. Struct. Geol.* **5**, 383–399.

Cowie, P. A. & Scholz, C. H. 1992a. Physical explanation for the displacement-length relationship of faults using a post-yield fracture mechanics model. *J. Struct. Geol.* **20**, 1133–1148.

Cowie, P. A. & Scholz, C. H. 1992b. Displacement-length scaling relationship for faults: data synthesis and discussion. *J. Struct. Geol.* **20**, 1149–1156.

Dahlen, F. A. 1984, Noncohesive critical Coulomb wedges: An exact solution. *J. geophys. Res.* **89**, 5389–5396.

Dahlen, F. A., Suppe, J. & Davis, D. 1984. Mechanics of fold-and-thrust belts and accretionary wedges. *J. geophys. Res.* **88**, 10,087–10,101.

Dahlstrom, C. D. A. 1969. Balanced cross-sections. *Can. J. Earth Sci.* **6**, 743–757.

Dahlstrom, C. D. A. 1970. Structural geology in the eastern margin of the Canadian Rocky Mountains. *Bull. Can. Petrol. Geol.* **18**, 332–406.

Davis, D., Suppe, J. & Dahlen, F. A. 1983. Mechanics of fold-and-thrust belts and accretionary wedges. *J. geophys. Res.* **88**, 1153–1172.

De Paor, D. 1987. STRAIN SAMPLER. Mac computer program. Department of Earth and Planetary Sciences, The John Hopkins University, Baltimore, MD, U.S.A.

Diegel, F. A. 1986. Topological constraints on imbricate thrust networks, examples from the Mountain City window, TN, U.S.A. *J. Struct. Geol.* **8**, 269–279.

Dixon, J. M. & Liu, S. 1992. Centrifuge modelling of the propagation of thrust faults. In: *Thrust Tectonics* (edited by McClay, K. R.). Chapman & Hall, London, U.K., 53–69.

Douglas, R. J. W. 1958a. Mount Head map area, Alberta. *Mem. geol. Surv. Can.* **291**,

Douglas, R. J. W. 1958b. Chungo Creek map-area, Alberta. *Geol. Surv. Can. Pap.* **53-3**.

Douglas, R. J. W. & Lebel, D. 1993. Geology and structure cross-section, Cardinal River, Alberta. *Geol. Surv. Can. Map.* 1828a, scale 1:50,000.

Elliott, D. 1976a. The energy balance and deformation mechanisms of thrust sheets. *Phil. Trans. R. Soc. Lond.* **283A**, 289–312.

Elliott, D. 1976b. The motion of thrust sheets. *J. geophys. Res.* **81**, 949–963.

Ellis, M. A. & Dunlap, W. J. 1988. Displacement variation along thrust faults: implications for the development of large faults. *J. Struct. Geol.* **10**, 183–192.

Gardner, D. A. C. & Spang, J. H. 1973. Model studies of the displacement transfer associated with overthrust faulting. *Bull. Can. Petrol. Geol.* **21**, 534–552.

Gillespie, P. A., Walsh, J. J. & Watterson, J. 1992. Limitations of dimension and displacement data from single faults and the consequences for data analysis and interpretation. *J. Struct. Geol.* **20**, 1157–1172.

Gretener, P. E. 1972. Thoughts on overthrust faulting in a layered sequence. *Bull. Can. Petrol. Geol.* **25**, 110–122.

Hake, B. F., Willis, R. & Addison, C. C. 1942. Folded thrust faults in the Foothills of Alberta. *Bull. geol. Soc. Am.* **53**, 291–334.

Harris, L. D. & Milici, R. D. 1977. Characteristics of thin-skinned style deformation in the southern Appalachians, and potential hydrocarbon traps. *U.S. Geol. Surv. Prof. Pap.* **108**.

Hossack, J. R. 1983. A cross-section through the Scandinavian Caledonides constructed with the aid of branch line maps. *J. Struct. Geol.* **5**, 103–111.

House, W. M. & Gray, D. R. 1982. Displacement transfer at thrust terminations in Southern Appalachians. *Bull. Am. Ass. Petrol. Geol.* **66**, 830–842.

Kanamori, H. & Anderson, D. L. 1975. Theoretical basis of some empirical relations in seismology. *Bull. seism. Soc. Am.* **65**, 1075–1095.

Langenberg, C. W. 1985. The geometry of folded and thrusted rocks in the Rocky Mountain Foothills near Grande Cache, Alberta. *Can. J. Earth Sci.* **22**, 1711–1719.

Lebel, D. 1993. Geometry, kinematics and computer simulations of thrust faulting, central Canadian Rocky Mountains, Alberta. Unpublished Ph.D. thesis, McGill University, Montréal, Québec, Canada.

Liu, S. & Dixon, J. M. 1991. Centrifuge modelling of thrust faulting: structural variation along strike in fold-thrust belts. *Tectonophysics* **188**, 39–62.

MacKay, B. R. 1940a. Pembina Forks. Geol. Surv. Can. preliminary geological Map 610A.

MacKay, B. R. 1940b. Grave Flats, Alberta. *Geol. Surv. Can. Pap.* **40-15**.

McEachran, D. B. 1985. Strain-graphics programs. Macintosh computer programs, Rockware, Inc., Denver, CO, U.S.A.

Mountjoy, E. W. 1960a. Structure and stratigraphy of the Miette and adjacent areas, eastern Jasper National Park, Alberta. Unpublished Ph.D. thesis, University of Toronto, Toronto, Canada.

Mountjoy, E. W. 1960b. Miette map-area. Geological Survey of Canada, Map 40-1959, scale 1:63,360.

Mountjoy, E. W., Price, R. A. & Lebel, D. 1992. Geology and structure cross-sections, Mountain Park, Alberta. Geological Survey of Map 1830A, scale 1:50,000.

Price, R. A. 1967. The tectonic significance of mesoscopic subfabrics in the southern Rocky Mountains of Alberta and British Columbia. *Can. J. Earth Sci.* **4**, 39–70.

Price, R. A. & Mountjoy, E. W. 1970. Geologic structure of the Canadian Rocky Mountains between Bow and Athabasca Rivers—a progress report. In: *Structure of the South Canadian Cordillera* (edited by Wheeler, J. O.). *Spec. Pap. geol. Ass. Can.* **6**, 7–25.

Price, R. A., Stott, D. F., Campbell, R. B., Mountjoy, E. W. & Ollerenshaw, N. C. 1977. Athabasca River. Geological Survey of Canada, Geological Atlas Series, Map 1339A, Scale 1:1, 000, 000.

Ramsay, J. G. & Huber, M. I. 1983. *The Techniques of Modern Structural Geology. Volume* 1: *Strain Analysis*. Academic Press Inc., London.

Rich, J. L. 1934. Mechanics of low-angle overthrust faulting as illustrated by Cumberland thrust block, Virginia, Kentucky and Tennessee. *Bull. Am. Ass. Petrol. Geol.* **1**, 1584–1596.

Sanderson, D. A. & Spratt, D. A. 1992. Triangle zone and displacement transfer structures in the Eastern Front Ranges, Southern Canadian Rocky Mountains. *Bull. Am. Ass. Petrol. Geol.* **76**, 828–839.

Sanderson, J. O. G. 1939. Geology of the Brazeau area. *Canadian Instit. Mining Metall. Trans.* **XLII**, 429–442.

Scholz, C. H., Aviles, C. A. & Wesousky, S. G. 1986. Scaling differences between large interplate and intraplate earthquakes. *Bull. seism. Soc. Am.* **76**, 65–70.

Scholz, C. H. 1990. *The Mechanics of Earthquakes and Faulting*. Cambridge University Press, Cambridge.

Schwartz, D. P. & Coopersmith, K. J. 1984. Fault behaviour and characteristic earthquakes: examples from the Wasatch and San Andreas fault zones. *J. geophys. Res.* **89**, 5681–5698.

Tysdal, R. G. 1986. Thrust faults and back thrusts in Madison Range of southwestern Montana foreland. *Bull. Am. Ass. Petrol. Geol.* **70**, 360–376.

Walsh, J. J. & Watterson, J. 1988. Analysis of the relationship between displacements and dimensions of faults. *J. Struct. Geol.* **10**, 239–247.

Wojtal, S. 1986. Deformation within foreland thrust sheets by populations of minor faults. *J. Struct. Geol.* **8**, 341–360.

APPENDIX A

Description of the spreading simple shear numerical model

The model is set in a Cartesian (xy) reference frame, with the axis of shortening along the x direction. The position of the new thrust trace (Fig. 2b) after each slip increment can be determined easily relative to the footwall position of the nucleation point of the fault, F_0 with coordinates (x_0, y_0), by tracking three key points, the position of the central point of maximum displacement at a specific slip increment, $F_c(N)$ and the left and right lateral fault tips at a new increment of displacement (respectively $F_L(N)$ and $F_R(N)$). The coordinates of each of these points are noted (x_c, y_c), (x_L, y_L) and (x_R, y_R). Hence after each new slip increment (N), the central point of maximum displacement will be at

$$F_c(N) = (x_c(N-1) + u_N, y_0) \quad \text{(A1)}$$

and the lateral tips will be at

$$F_L(N) = (x_0, y_0 - (k \cdot u_N)) \quad \text{(A2)}$$

$$F_R(N) = (x_0, y_0 + (k \cdot u_N)), \quad \text{(A3)}$$

since displacement vectors are parallel to the x axis but of unequal length. By determining ϕ_1 and ϕ_2 (Fig. 2b), the displacement vector for each shear plane (S) along the thrust width is found through

$$u_N(S) = x_s(N) - x_s(N-1) \quad \text{(A4)}$$

where (x_s, y_s) are the coordinates of each point $F_s(N)$ along the thrust before ($N-1$) and after a new slip increment (N). Left of $F_c(N)$ these are:

$$x_s(N) = \tan\phi_1 \cdot (y_s - y_R(N)) \quad \text{(A5)}$$

$$x_s(N-1) = \tan\phi_2 \cdot (y_s - y_R(N-1)) \quad \text{(A6)}$$

and right of $F_c(N)$

$$x_s(N) = \tan\phi_1 \cdot (y_L(N) - y_s) \quad \text{(A7)}$$

$$x_s(N) = \tan\phi_2 \cdot (y_L(N-1) - y_s). \quad \text{(A8)}$$

Naturally, the value of x_s is set to 0 before each new slip increment, left of $y_L(N)$ and right of $y_R(N)$.

APPENDIX B

Operation of the THREE THRUSTS computer program

The execution of the program can be started and interrupted at any time. A series of lines with a spacing defined by the operator are drawn on the computer screen as strain markers. An option permits one to paste in any bitmap image as an alternative marker, or starting pattern (e.g. an image generated from a previous simulation with locked thrusts). The user can choose between one and three thrusts that can be active during the execution of the simulation. The default parameters that define the fault propagation rate can be changed, that is the values of k and a (see Table 1 and Walsh & Watterson 1988).

If three thrust faults are set, the program first finds the location of the nucleation points as selected by the user and then proceeds to rank them relative to their position from the bottom of the computer screen (foreland). The lowermost one is T1 (nearest the foreland or of first rank), the one closest to the rear boundary is T3 (Fig. 3). The program will not allow two thrust nucleation points to be placed on the same row of pixels. THREE THRUSTS then proceeds to calculate and draw on the computer screen each slip increment for each fault, one fault at a time. Since the three thrusts are developing synchronously, each one slipping by minute increments, the order in which each fault moves is not significant except for some special cases (faults propagating on same axis). Arbitrarily, the program starts with the first increment of deformation on T1, doing T2, T3 in turn and then back to T1, repeating this cycle until the user stops it. An alternate mode (manual mode) permits one to choose a preferred fault to be activated by simply clicking on it. The program keeps track of each increment of faulting independently for each fault (e.g. in a three thrust scenario, the user might choose to activate T3 a number of times before the first slip on T1, then make any choices with any of the three faults).

The first and subsequent increments of displacement on each fault are calculated, together with new locations, using their maximum displacement center point and lateral thrust tips. The model is scaled so that the rate of propagation of a fault is related to its width according to the equations of Walsh & Watterson (1988), which describe natural faults of various scales and rocks of various material properties. The model outlined here is mainly useful for faults of kilometer-scale lateral width, but various situations can be modeled since any scale can be used for the simulations. The default scale of the model is 100 m per pixel (1 pixel = 1/72 inch). Hence in this case, each increment of displacement of 100 m or more is calculated at the center of the fault, the column of pixels behind this point is displaced by an equivalent number of pixels. The incremental displacement is then distributed with a linear decrease in value on each column of pixels found left and right of the center of the thrust to the new thrust tip where the increment displacement is nil according to the spreading simple shear mechanism (Fig. 2).

The location of each pixel composing the leading edge of each fault, relative to the reference grid, is kept in a positioning matrix (x–y coordinates) so that the strain effect on a hinterland thrust being transposed piggyback by a frontal thrust is always tracked. A hinterland thrust which has changed its position relative to the reference grid can thus be deformed subsequently at its correct new location. Because each foreland thrust applies incremental transport of varying value along strike onto overlapping hinterland thrusts, the location of the affected hinterland thrusts has to be followed independently from the computer screen output, within the positioning matrix. The shape of a hinterland thrust trace will change with the overlap and piggyback transport by a foreland thrust and will not conform to a simple bi-rectilinear V like the one shown for a single fault (Fig. 2). The positioning matrix is thus used by the program so that the same vectorial addition to each pixel column behind the thrust trace is performed as if both fault segments were rectilinear, thus neglecting the effect of shape change on the kinematics (Fig. 4). The coordinates of the positioning matrix also allow the program to keep track of the axis of lateral spreading of each thrust tip (Fig. 2a).

Special cases

Special situations are handled using test routines in order to prevent the model from producing graphical aberrations that would not be comparable to geologic phenomena. When such special circumstances occur, the program follows corresponding empirical rules. These empirical rules are derived from current knowledge of thrust faults behavior in thrust-fold belts and have been determined while programming, as answers to problematic situations that happened as the code was being tested. Two special cases are discussed below.

Special case 1: *T3 thrust tip propagating ahead of T2 thrust tip.* Because of the cumulative layer-perpendicular shear strain developed behind a propagating foreland thrust fault (T1), the rear-most fault (or nearest the hinterland, T3) within the strain zone will be deformed and may eventually grow to a position where one of its tips will be ahead of

a tip of T2 (Fig. 5c). To spot this situation, the program always verifies if the new thrust tip of T3 occupies such a position relative to T2. If so, the program takes note and executes the subsequent deformations so that T3 carries T2 piggyback (i.e. T2 will hide parts of T3 if it moves over it).

Special case 2: *Intersecting thrust traces*. During its evolution, a thrust fault may propagate into (or merge with) another fault. In this case, THREE THRUSTS detects the situation and checks if the propagating fault is in the hangingwall or footwall of the other one. If the propagating fault is situated in the footwall, the image created on the computer screen will be a simulation of piggyback thrusting and merging with the overlying fault, so the thrust trace will not cross-cut the hangingwall fault; in cross-section this situation would appear as a duplex (Dahlstrom 1970, Boyer & Elliott 1982). The program takes note of the situation for all future moves of both faults (T1 carries T2, Fig. 7a). Another special case may arise if the propagating thrust (T2) has been sufficiently strained by T1 to occur ahead of the lateral tips of T1 (Figs. 7b1 & b2). In this case, the propagating fault T2 cannot cut through the intersecting fault T1 because it is constrained within the T1 thrust sheet and thus must tear off the part of T1 situated to the right of the branch point, point X (Fig. 7b2 see below for further discussion). T2 then follows the former axis of lateral thrust propagation of T1 (compare the growth of T2 from Fig. 7b2 to Fig. 7b3).